Polyhedron 204 (2021) 115267

Contents lists available at ScienceDirect

Polyhedron

journal homepage: www.elsevier.com/locate/poly

A family of salamo-type trinuclear Co(II) and Ni(II) complexes: Structural characterization, Hirshfeld surface analysis and fluorescent properties

Peng Li, Shi-Zhen Li, Yu-Xin Wei, Wen Kui Dong *

School of Chemistry and Chemical Engineering, Lanzhou Jiaotong University, Lanzhou 730070, PR China

ARTICLE INFO

Article history:
Received 20 March 2021
Accepted 11 May 2021
Available online 17 May 2021

Keywords:
Salen-type ligand
Complex
Crystal structure
Hirshfeld surface analysis
Fluorescence property

ABSTRACT

Three trinuclear complexes, [{CoL(MeOH)(μ-OAc)}$_2$Co] (**1**), [{CoL(EtOH)(μ-OAc)}$_2$Co]·2CH_3CH_2OH (**2**) and [{NiL(MeOH)(μ-OAc)}$_2$Ni]·2CH_3OH (**3**) have been successfully synthesized by wet-chemical method using asymmetric salamo-based polydentate chelating ligand (H_2L) with transition metal(II) acetate ($Co(OAc)_2·4H_2O$ or $Ni(OAc)_2·4H_2O$). The ligand H_2L with N_2O_2 coordination cavity can accommodate transition metals, at the same time, the oxygen atoms of the phenolic hydroxyl groups can bridge the metal atoms to obtain muiltnuclear metal complexes. There are inversion centers in complexes **1**–**3** and all M (II) atoms possess six-coordinated distorted octahedral geometries. Complexes **1** and **3** are further assembled into extended two-dimensional supramolecular via intermolecular interactions, but complex **2** forms three-dimensional supramolecular structure. The interactions were quantitatively determined by Hirshfeld surfaces analyses. Significantly, complexes **1**–**3** have been characterized by elemental analyses, IR spectra, UV–Vis spectroscopy and X-ray crystallography analyses. Fluorescence properties were also investigated.

1. Introduction

Coordination chemistry has been active in various fields of chemistry, and has become an important branch of chemistry [1]. Over the years, salen-bases played an important role as chelating ligands in the coordination chemistry of main group, transition metals and rare earth [2]. The complex units formed by salen and its analogues are the basic building blocks for supramolecular structures and coordination polymers, which is an important part of the diversity of the complexes [3]. The tetradentate salen-base ligands and their transition metal complexes have been extensively studied in the fields of catalytic reactions [4], optical materials and biochemistry [5], and continue to expand their research fields in breadth and depth. Salen and its related N_2O_2 polydentate chelating ligands are usually prepared by gently heating the mixed solution of diamines and salicylaldehyde and its derivatives [6]. However, due to the instability of imine bond, which is not possible obtain a single compound with two or more N_2O_2-donor cavities [7]. Through the years, in the field of coordination chemistry, a new type of salen-based analogue, salamo-based compounds (R-CH = N—O-$(CH_2)_n$—O—N = CH-R) have been developed [8]. Because the strong electronegativity of oxygen atoms, which can significantly affect the electron density distribution of ligands and control the reversible reaction of imine bonds, we can use unstable and stable building blocks to describe the compounds based on salen- and salamo-based compounds [9]. Through coordination-driven self-assembly, various 3d [10], 3d-s [11], 3d-4f [12] homometal-multinuclear, hetermetal-multinuclear complexes and coordination polymers have been developed based on symmetric and asymmetric salamo-based ligands. Nowadays, the synthesis of salamo-based polydentate chelating ligands [13], complexes [14] and molecular probes [15] with excellent properties and specific structures, as well as the exploration of potential applications in various fields, have become part of the field of coordination chemistry. Nabeshima's group has done a lot of excellent researches on salamo-based ligands and their corresponding macrocyclic complexes, chiral complexes and the selective introduction of different metal ions in different cavities [16].

Here, we designed and synthesized a new asymmetric polydentate chelating ligand H_2L with N_2O_2 donor and three M(II) complexes **1**–**3** [3f–3i]. Through coordination-driven self-assembly and quantitative analysis of Hirshfeld surface, the interactions between complex units have been studied, and the fluorescence properties have also been explored.

* Corresponding author.
E-mail address: dongwk@126.com (W.K. Dong).

https://doi.org/10.1016/j.poly.2021.115267
0277-5387/

2. Experimental section

2.1. Materials and instrumentation

5-Nitrosalicylic aldehyde (98%), 2-hydroxy-4-methoxybenzaldehyde (98%), *N*-Hydroxyphthalimide (98%) and 1,2-dibromoethane (99%) were purchased from Meryer and used without further purification, hydrazine hydrate (≥80%) was purchased from YUMEI and used without further purification. The solvents and reagents were analytical grade reagents. C, H and N analyses were performed via a GmbH VarioEL V3.00 automatic elemental analyses instrument. ^{1}H NMR spectra were recorded using a Bruker AVANCE DRX-400 spectrometer (Bruker AVANCE, Billerica, MA, USA). Melting points were made via microscopic melting point instrument made in Beijing Tektronix Instruments Limited Company. FT-IR spectra were gained via a VERTEX70 FT-IR spectrophotometer, with samples prepared as KBr (4000–400 cm^{-1}) pellets. UV–Vis absorption spectra were obtained via a Shimadzu UV-2550 spectrometer. X-ray single crystal structures were carried out on a Bruker D8 Venture diffractometer. Fluorescence spectrum were measured via an F-7000 FL spectrophotometer.

2.2. Synthesis and characterization of H_2L

The synthesis of 1,2-bis(aminooxy)ethane is shown in scheme 1, please refer to the original literatures [8].

The synthetic routes of 2-[*O*-(1-ethyloxyamide)]oxime-4-nitrophenol and H_2L are shown in scheme 1. 2-[*O*-(1-Ethyloxyamide)] oxime-4-nitrophenol was prepared by the solution of 5-nitrosalicylic aldehyde (3 mmol, 506.1 mg) in ethanol (60 mL) was added to a solution of 1,2-bis(aminooxy)ethane (6 mmol, 552.36 mg) in ethanol (10 mL), the mixed solution was reacted for 4 h. The solution was concentrated in *vacuo* and the residue was purified by column chromatography (SiO_2, dichloromethane /ethyl acetate = 15:1), 2-[*O*-(1-ethyloxyamide)]oxime-4-nitrophenol was collected by concentrated in *vacuo*. Yield: 41.1%. *Anal.* Calc. for $C_9H_{11}N_3O_5$: C, 44.82; H, 4.60; N, 17.42. Found: C, 44.75; H, 4.65; N, 17.26%. ^{1}H NMR (500 MHz, $CDCl_3$): δ 10.73 (s, 1H), 8.27 (s, 1H), 8.18 (dd, *J* = 9.1, 2.7 Hz, 1H), 8.14 (d, *J* = 2.7 Hz, 1H), 7.07 (d, *J* = 9.1 Hz, 1H), 5.54 (s, 2H), 4.44–4.41 (m, 2H), 4.01–3.98 (m, 2H).

The ligand H_2L was synthesized by the rection of 2-[*O*-(1-ethyloxyamide)]oxime-4-nitrophenol (241.1 mg, 1.0 mmol) in ethanol (10 mL) with 2-hydroxy-4-methoxybenzaldehyde (152.1 mg, 1.0 mmol) in ethanol (10 mL). The solutions were stirred for 1 h. Light pink precipitates were filtered, washed by a small amount of ethanol and dried in *vacuo*. Yield: 78.6%. m. p.: 131–132 ℃ .*Anal.* Calc. for $C_{17}H_{17}N_3O_7$: C, 54.40; H, 4.57; N, 11.20. Found: C, 54.95; H, 4.33; N, 11.03%. ^{1}H NMR (500 MHz, $CDCl_3$): δ 10.66 (s, 1H), 9.90 (s, 1H), 8.31 (s, 1H), 8.22–8.19 (m, 1H), 8.19–8.16 (m, 2H), 7.08 (d, *J* = 3.7 Hz, 1H), 7.07 (d, *J* = 3.2 Hz, 1H), 6.52 (d, *J* = 2.4 Hz, 1H), 6.50 (dd, *J* = 8.5, 2.5 Hz, 1H), 4.55 (dt, *J* = 6.3, 3.6 Hz, 2H), 4.49 (dt, *J* = 4.0, 3.6 Hz, 2H), 3.84 (s, 3H).

2.3. Synthesis of complex **1**

To 2 mL of $CHCl_3$/ CH_3CN mixed solution (v/v = 1: 1) of H_2L (3.75 mg, 0.01 mmol) was added 4 mL of MeOH solution of Co$(OAc)_2{\cdot}4H_2O$ (2.90 mg, 0.01 mmol), which immediately turned to light brown. The brown block-shaped single crystals suitable for X-ray crystallographic analysis was obtained by kept undisturbed crystallization at room temperature with evaporating part of the solution. Finally, washed with methanol, and then dried at ambient temperature. Yield: 45%, based on Co$(OAc)_2{\cdot}4H_2O$. Anal. Calc. for $C_{40}H_{44}Co_3N_6O_{20}$ (%): C, 43.45; H, 4.01; Co, 15.99; N, 7.60. Found: C, 43.85; H, 3.82; Co, 15.36; N, 7.33.

2.4. Synthesis of complex **2**

The same method as complex **1** was used. To 2 mL of $CHCl_3$/ CH_3CN mixed solution (v/v = 1: 1) of H_2L (3.75 mg, 0.01 mmol) was added 4 mL of EtOH solution of Co$(OAc)_2{\cdot}4H_2O$ (2.90 mg, 0.01 mmol). Yield: 43%, based on Co$(OAc)_2{\cdot}4H_2O$. Anal. Calc. for $C_{46}H_{60}Co_3N_6O_{22}$ (%): C, 45.07; H, 4.93; Co, 14.42; N, 6.86. Found: C, 45.36; H, 4.82; Co, 14.09; N, 6.44.

2.5. Synthesis of complex **3**

Ni$(OAc)_2{\cdot}4H_2O$ (2.50 mg, 0.01 mmol) was dissolved in 3 mL of ethanol, a solution of H_2L (3.80 mg, 0.01 mmol) in $CHCl_3/CH_3CN$ mixed solution (v/v = 1: 1) was added to it, which immediately turned to light green. Finally, the harvested green crystals were washed with ethanol. Yield: 49%, based on Ni$(OAc)_2{\cdot}4H_2O$. Anal. Calc. for $C_{42}H_{52}N_6Ni_3O_{22}$ (%): C, 43.15; H, 4.48; Ni, 15.06; N, 7.19. Found: C, 43.46; H, 4.12; Ni, 14.79; N, 6.94.

2.6. Crystal structure determination

X-ray diffraction data of complexes **1**–**3** were collected on a Bruker D8 Venture diffractometer with graphite-monochromatized Mo-Kα radiation (λ = 0.71073 Å). Complexes cooled in a nitrogen gas cryostream to 173 K. The complexes structures were solved by intrinsic phasing using the SHELXT [17], refinement was performed in Olex2 with SHELXL-2018 by least-squares minimization against F^2 [18a,18b]. Data were corrected for absorption effects using the empirical multi-scan method (SADABS) [18c]. The

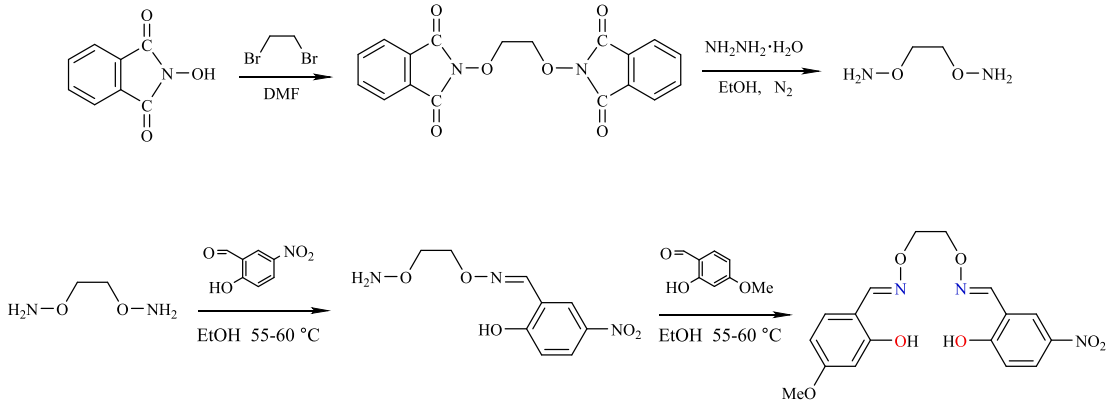

Scheme 1. Synthetic routes to 1,2-bis(aminooxy)ethane and the ligand H_2L.

nonhydrogen atoms were refined with anisotropic thermal parameters. All the hydrogen atoms were geometrically fixed and allowed to refine using a riding model. Complex **1** has high positive value of 1.41 e.A^{-3} in the final difference map, which is next to Co1 of complex **1**. For structures containing heavy atoms, the peak/valley maximums are usually larger, and these residual peaks are usually in the range of about 60–120 pm (0.6–1.2 Å) from the heavy atoms. If the atomic number of the heavy atom is Z, these electron density peaks or valleys can be considered reasonable in the range of ± 0.1Z × 10^{-6} e pm^{-3} (±0.1Z eÅ^{-3}). The experimental details for the structural determination are presented in Table 1. Selected bond lengths (Å) and angles (°) for complexes **1**–**3** are presented in Table 2.

3. Results and discussion

3.1. Spectral investigation

3.1.1. IR spectra

The infrared spectra of the ligand H_2L and its trinuclear complexes were recorded in the range of 400–4000 cm^{-1} (Fig. 1). The O—H stretching vibration band of the ligand was observed at 3425 cm^{-1} [9a], this band was disappeared in the IR spectra of complexes **1**–**3**, which is indicative of the fact that the phenolic OH groups of H_2L have been deprotonized and coordinated to the Co(II) or Ni(II) atoms [12c]. Besides, absorption bands at about 3428, 3426 and 3426 cm^{-1} in complexes **1**–**3** could be ascribed to the –OH groups of existed methanol or ethanol molecules, respectively, which are also confirmed with the X-ray crystallography analyses [10a]. The C=N groups of the ligand have an obvious stretching vibration band at about 1608 cm^{-1}, but in the complexes **1**–**3**, the stretching vibration bands of C=N appears at about 1603, 1607 and 1606 cm^{-1} and shifted to low frequencies, which indicates that the M(II) atoms are coordinated with the N atoms of the C=N groups [10b]. Moreover, the Ar-O stretching vibration band of ligand is observed at approximately 1285 cm^{-1}, but complexes **1**–**3** appear at 1215, 1217 and 1213 cm^{-1}, obviously shifted to lower frequencies, which indicated that the M(II) atoms are coordinated with the O atoms of the aromatic rings [12b]. At the same time, in order to distinguish the M–N and M–O bonds, complexes infrared spectrum have been carried out a careful study, the stretching vibration bands appeared at 556, 583 and 562 cm^{-1} in the M(II) complexes could be attributed to ν(Cu–N) bonds, meanwhile, the bands appeared at 478, 472, and 479 cm^{-1} were indicated ν(Cu–O) bonds [12d].

3.1.2. UV–Vis spectroscopy

The UV–Vis spectroscopy of the ligand and complexes **1**–**3** were recorded at ambient temperature, which was dissolved in ethanol with the concentration were 1 × 10^{-5} mol/L. As shown in Fig. 2a, three successive peaks at *ca.* 231, 273 and 304 nm were observable. The absorption peaks at 231 and 273 nm could be attributed to the π-π* charges transition of aromatic rings [10a], and the later peak at 304 nm could be identified as π-π* charges transition of C=N groups [13a]. Compared with the UV–Vis absorption peaks of the ligand, the spectrums of complexes changed obviously (Fig. 2b).

The titration curves are given in Fig. 2c and Fig. 2d. The titration curves of complexes **1** and **2** are given in Fig. 2c, compared with the free ligand H_2L (1 × 10^{-5} mol/L), with the concentration of Co^{2+} (1 × 10^{-3} mol/L) increase gradually, two new peaks have been discovered at about 247 and 363 nm, but absorption peaks of ligand at 231 and 273 nm disappear, which indicted Co^{2+} ions have coordination with L^{2-} units. Significantly, when the concentration of Co^{2+} ions reach 1.5 equivalents, the absorption intensity of the UV–Vis absorption spectrums become stable, which indicated the stoichiometry of Co^{2+} and H_2L is 1.5 : 1 and consistent with X-ray crys-

Table 1
Crystallographic data and refinement parameters for complexes **1**, **2** and **3**.

Complex	**1**	**2**	**3**
Empirical formula	$C_{40}H_{44}Co_3N_6O_{20}$	$C_{46}H_{60}Co_3N_6O_{22}$	$C_{42}H_{52}N_6Ni_3O_{22}$
Formula weight	1105.60	1225.79	1169.02
Temperature (K)	173.0	173.0	173.0
Wavelength (Å)	0.71073	0.71073	0.71073
Crystal system	monoclinic	triclinic	triclinic
Space group	$P2_1/n$	P-1	P-1
Unit cell dimension			
a (Å)	10.7988(7)	8.9588(3)	10.4177(3)
b (Å)	15.3763(11)	10.9065(4)	10.8117(3)
c (Å)	13.3942(10)	14.2696(5)	10.9671(4)
α (°)	90	70.6270(10)	101.2700(10)
β (°)	95.184(3)	79.8900(10)	100.7990(10)
γ (°)	90	76.3070(10)	94.0630(10)
V (Å^3)	2215.0(3)	1270.76(8)	1182.56(6)
Z	2	1	1
D_{calc} (g · cm^{-3})	1.658	1.602	1.642
μ (mm^{-1})	1.200	1.057	1.273
F(000)	1134.0	635.0	606.0
Crystal size (mm)	0.16 × 0.14 × 0.13	0.21 × 0.19 × 0.17	0.19 × 0.17 × 0.14
θ range (°)	4.622 to 53.644	5.328 to 53.626	4.852 to 53.47
Index ranges	$-13 \le h \le 13, -17 \le k \le 17, -20 \le l \le 20$	$-11 \le h \le 11, -18 \le k \le 18, -19 \le l \le 19$	$-13 \le h \le 13, -15 \le k \le 15, -17 \le l \le 17$
	$-19 \le k \le 19$	$-13 \le k \le 13$	$-13 \le k \le 13$
	$-16 \le l \le 16$	$-18 \le l \le 18$	$-13 \le l \le 13$
Reflections collected	26,304	23,613	14,395
Independent reflection	4709 [R_{int} = 0.0792]	5411 [R_{int} = 0.0583]	5021 [R_{int} = 0.0317]
Completeness to (%) (θ)	99.3	99.4	99.8
Data/restraints/parameters	4709/1/320	5411/9/367	5021/4/339
Final R_1, wR_2 indices [$I > 2\sigma(I)$]	0.0624, 0.1569	0.0357, 0.0913	0.0319, 0.0720
$2\sigma(I)$]			
R_1, wR_2 indices (all data)	0.0730, 0.1656	0.0485, 0.0968	0.0404, 0.0771
GOF	1.055	1.034	1.066
$\Delta\rho_{max,min}$ (e Å^{-3})	1.41/-0.98	0.58/-0.53	0.37/ −0.45

Table 2
Selected bond lengths (Å) and angles (°) for complexes **1**–**3**.

Complex 1		**Complex 2**		**Complex 3**	
Co1-O1	2.080(3)	Co1-O1	2.0460(15)	Ni1-O1	2.0225(15)
Co1-N2	2.160(3)	Co1-N2	2.1216(19)	Ni1-N2	2.0605(19)
Co1-N3	2.122(3)	Co1-N3	2.058(2)	Ni1-N3	2.0277(19)
Co1-O6	2.042(3)	Co1-O6	2.0438(15)	Ni1-O6	2.0153(15)
Co1-O9	2.059(3)	Co1-O9	2.0638(16)	Ni1-O9	2.0313(16)
Co1-O8	2.168(3)	Co1-O8	2.1932(18)	Ni1-O8	2.0994(16)
Co2-O1	2.133(3)	Co2-O1	2.1535(15)	Ni2-O1	2.1434(14)
Co2-O6	2.107(3)	Co2-O6	2.1222(15)	Ni2-O6	2.0640(15)
Co2-O10	2.049(3)	Co2-O10	2.0337(15)	Ni2-O10	2.0578(15)
O1-Co1-N2	84.86(12)	O1-Co1-N2	86.19(7)	O1-Ni1-N2	88.35(7)
O1-Co1-N3	166.62(12)	O1-Co1-N3	167.04(8)	O1-Ni1- N3	168.02(7)
O1-Co1-O8	88.49(11)	O1-Co1-O8	85.85(7)	O1-Ni1- O8	86.27(6)
N2-Co1-O8	83.48(12)	N2-Co1-O8	85.41(7)	N2-Ni1- O8	85.01(7)
N3-Co1-N2	107.50(13)	N3-Co1-N2	100.79(8)	N3-Ni-N2	99.90(8)
N3-Co1-O8	87.91(12)	N3-Co1-O8	84.17(9)	N3-Ni- O8	85.82(7)
O6-Co1-O1	86.35(12)	O6-Co1-O1	82.15(6)	O6-Ni- O1	81.30(6)
O6-Co1-N2	164.60(12)	O6-Co1-N2	168.16(7)	O6-Ni-N2	169.59(7)
O6-Co1-N3	86.35(12)	O6-Co1-N3	90.23(7)	O6-Ni1-N3	90.95(7)
O6-Co1-O9	93.75(11)	O6-Co1-O9	89.05(6)	O6-Ni1-O9	87.32(6)
O6-Co1-O8	90.53(11)	O6-Co1-O8	91.61(6)	O6-Ni1-O8	95.38(6)
O9-Co1-O1	93.11(11)	O9-Co1-O1	95.50(6)	O9-Ni1-O1	93.02(6)
O9-Co1-N2	92.60(12)	O9-Co1-N2	94.13(7)	O9-Ni1-N2	92.13(7)
O9-Co1-N3	91.43(12)	O9-Co1-N3	94.87(8)	O9-Ni1-N3	95.31(7)
O9-Co1-O8	175.62(11)	O9-Co1-O8	178.84(6)	O9-Ni1-O8	177.07(7)
O1-Co2-O1$^{\#1}$	180.0	O1-Co2-O1$^{\#1}$	180.0	O1-Ni2-O1$^{\#1}$	180.0
O6$^{\#1}$-Co2-O1	101.89(10)	O6$^{\#1}$-Co2-O1	102.13(6)	O6$^{\#1}$-Ni2- O1	102.64(6)
O6-Co2-O1	78.11(10)	O6-Co2-O1	77.87(6)	O6-Ni2-O1	77.36(6)
O6-Co2-O6$^{\#1}$	180.0	O6-Co2-O6$^{\#1}$	180.0	O6-Ni2-O6$^{\#1}$	180.00
O10$^{\#1}$-Co2-O1	92.05(11)	O10$^{\#1}$-Co2-O1	91.95(6)	O10$^{\#1}$-Ni2-O1	91.86(6)
O10-Co2-O1	87.95(11)	O10-Co2-O1	88.41(6)	O10-Ni2-O1	88.14(6)
O10-Co2-O1$^{\#1}$	92.05(11)	O10-Co2-O1$^{\#1}$	91.95(6)	O10-Ni2-O1$^{\#1}$	91.86(6)
O10-Co2-O6	89.15(11)	O10-Co2-O6	88.01(6)	O10-Ni2-O6	89.15(6)
O10$^{\#1}$-Co2-O6	90.84(11)	O10$^{\#1}$-Co2-O6	91.99(6)	O10$^{\#1}$-Ni2-O6	90.49(6)
O10-Co2-O10$^{\#1}$	180.0	O10-Co2-O10$^{\#1}$	180	O10-Ni2-O10$^{\#1}$	180.00(5)

Symmetry code: $^{\#1}$ = 1-X, 1-Y, 1-Z.

tallographic analysis [11]. The titration curves of complex **3** is similar to that of the former two (Fig. 2d), with the concentration of Ni^{2+} (1×10^{-3} mol/L) increase gradually, the 273 and 340 nm absorption peaks of the free ligand gradually decrease and disappear, and new absorption peaks appear at 252 and 374 nm, which indicates that Ni^{2+} ions have coordinated with L^{2-} units and affect the charge transfer transition [12d]. Moreover, the absorption peak of complex **3** at 239 nm is red-shifted by 8 nm compared with the free ligand at 231 nm.

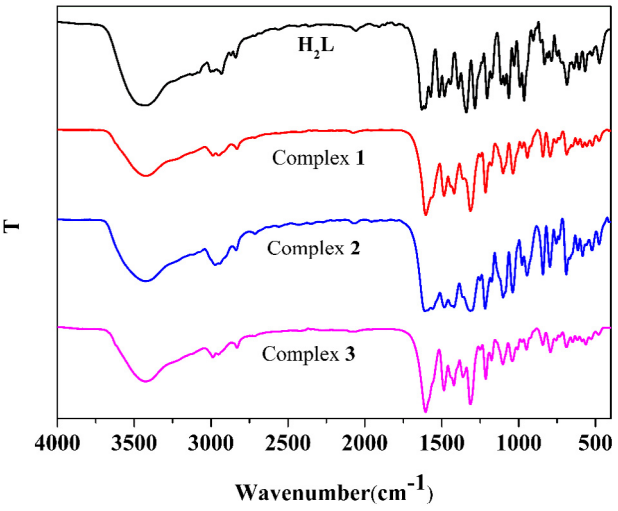

Fig. 1. IR spectra of H_2L and its corresponding complexes **1**–**3** (cm^{-1}).

3.2. Description of the crystal structures

3.2.1. The crystal structure and supramolecular interactions of complex *1*

Complex **1** possesses inversion center and crystallizes in the monoclinic crystal system (Fig. 3a), the crystal structure analysis shows that complex **1** is homo-trinuclear complex and the formula is [{CoL(MeOH)(μ-OAc)}$_2$Co]. Two ligand units $(L)^{2-}$ package three metal atoms, the μ-OAc^{-1} of the counter anions bridge two adjacent metal Co(II) atoms, and the terminal Co(II) atoms are coordinated with the solvent molecules at axially available position, so that all Co(II) atoms are six-coordinated (Fig. 3b). Co(II) atom (Co2) is located in the O6 coordination cavity, the equatorial sites around the Co2 occupied by the donor atoms O1, O6, O1$^{\#1}$ and O6$^{\#1}$ of the ligand $(L)^{2-}$ units, the axial positions are the oxygen atoms (O10 and O10$^{\#1}$) of the μ-OAc^{-} counter anions. The terminal Co(II) atoms (Co1) is located in the N_2O_4 cavity, N3, N7, O6 and O1 atoms come from N_2O_2 cavity to form equatorial plane, as well as, the axial positions are occupied by the oxygen atoms of solvent molecules (O8) and counter ions (O9), respectively. The trinuclear Co(II) complex reported by the Datta group, through the μ-N_3^- anion to connect the metal Co(II) atoms to form a trinuclear Co (II) complex [3f]. In 2019, the Andruh group reported a novel trinuclear Co(II) complex constructed from Mannich-schiff-base ligands [3g], there are different from that reported in this article.

In order to better explore the stacking trend of complexes, intramolecular and intermolecular interactions have been studied. Each complex unit have three intramolecular hydrogen bonds (C9-HAB···O9, *C*2-H2···O10$^{\#1}$ and C13-H13···O10$^{\#1}$) (Fig. 3c). At the same time, two intermolecular hydrogen bonds (O8$^{\#1}$-H8$^{\#1}$···O3$^{\#2}$ and C8-H8A···O2$^{\#3}$) and two π-related interactions (N1$^{\#2}$-O3$^{\#2}$-

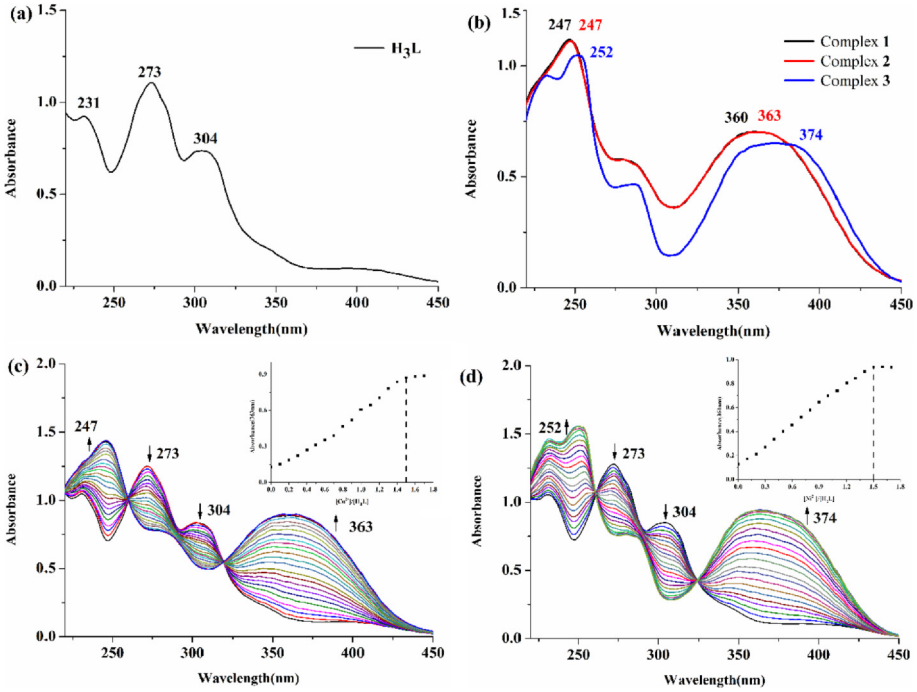

Fig. 2. (a) UV–vis spectrum of H_2L (1×10^{-5} M). (b) UV–vis spectra of complexes **1**–**3** (1×10^{-5} M). (c) The changes in H_2L (1×10^{-5} M) upon addition of Co^{2+} (1×10^{-3} M). Inset: the absorbance at 363 nm varies with the interaction of $[Co^{2+}]/[H_2L]$. (d) The changes in H_2L (1×10^{-5} M) upon addition of Ni^{2+}. Inset: the absorbance at 361 nm varies with the interaction of $[Ni^{2+}]/[H_2L]$.

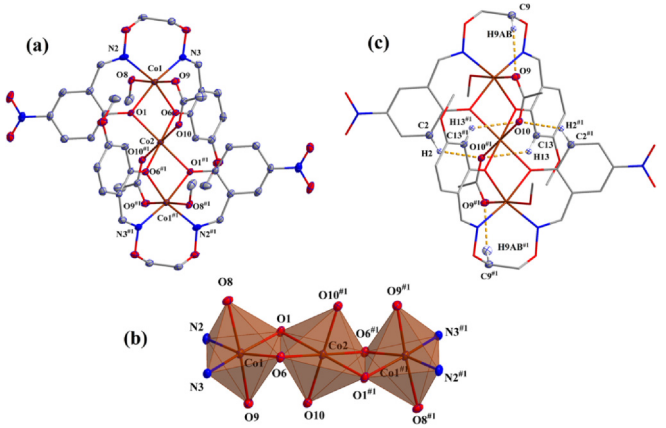

Fig. 3. (a) Molecule structure of complex **1**, ellipsoids are shown at the 30% probability level for reasons of clarity, symmetry code: $^{\#1}$ = 1-x, 1-y, 1-z. (b) Coordination polyhedrons for Co(II) atoms, symmetry code: $^{\#1}$ = 1-x, 1-y, 1-z. (c) View of the intramolecular hydrogen bonds, symmetry code: $^{\#1}$ = 1-x, 1-y, 1-z. Hydrogen atoms are omitted for clarity.

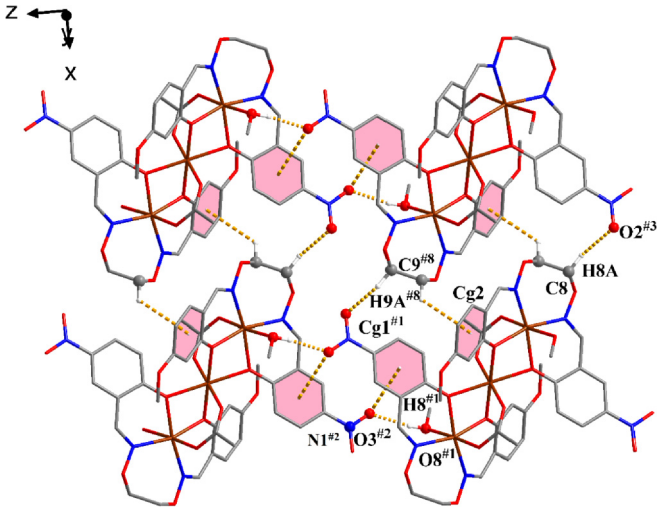

Fig. 4. View of the two-dimensional supramolecular structure of complex **1**. Intermolecular hydrogen bonds ($O8^{\#1}$-$H8^{\#1}$···$O3^{\#2}$ and C8-H8A···$O2^{\#3}$) and π-related interactions ($N1^{\#2}$-$O3^{\#2}$···$Cg1^{\#1}$ and $C9^{\#8}$-$H9A^{\#8}$···Cg2, Cg1 are the centroids of atoms C1/C2/C3/C4/C5/C6. Cg2 is the centroids of atoms C11/C12/C13/C14/C15/C16.) of complex **1**, symmetry code: $^{\#1}$ = 1-x, 1-y, 1-z; $^{\#2}$ = 1-x, 1-y, -z; $^{\#3}$ = -1 + x, y, z; $^{\#8}$ = -x, 1-y, 1-z. Hydrogen atoms are omitted for clarity.

···$Cg1^{\#1}$ and $C9^{\#8}$-$H9A^{\#8}$···Cg2) coordinate the complex units to form two-dimensional supramolecular structure [1f,2g,24] (Fig. 4). From the supramolecular structure of complex **1**, we can know that the oxygen atom of nitro group plays a key role in it. Putative hydrogen bond interactions and geometrical parameters for the π-related interactions of complexes **1**–**3** are shown in Table 3 and Table 4, respectively.

*3.2.2. The crystal structure and supramolecular interactions of complex **2***

Complex **2** possesses inversion center and crystallizes in the triclinic crystal system, the formula is $[\{CoL(EtOH)(\mu\text{-}OAc)\}_2Co]\cdot 2CH_3CH_2OH$. Compared with complex **1**, the coordination solvent molecules at the axial position of the terminal Co(II) atoms of complex **2** are different from that of complex **1**, and there are crystalline solvent molecules at the same time (Fig. 5a, 5b). The oxygen atoms of oxime group (O5, N3 and C10) are disordered unequally over two different positions (O5 and O5A, 0.617(6) and 0.383(6)), which are allowed for during refinement [10a].

In the structure of complex **2**, four intramolecular hydrogen-bondings (*C*2-H2···$O10^{\#1}$, C8-H8A···O9, C13-H13···$O1^{\#1}$ and C18-H18A···$O10^{\#1}$) and one intramolecular π-related interactions (C19-H19C···Cg1) were found, which plays a vital role in the structural stability of the complex unit (Fig. 5c). Simultaneously, one

Table 3
Putative hydrogen bond interactions (Å) for complexes **1**–**3**.

Complex **1**					
D–X···A	d(D–X)	d(X···A)	d(D···A)	∠D–X···A	Symmetry code
O8$^{\#1}$-H8$^{\#1}$···O3$^{\#2}$	0.83(3)	1.96(3)	2.749(4)	158(6)	1-x, 1-y, -z
C9-H9AB···O9	0.99	2.46	3.335(5)	148	
*C*2-H2···O10$^{\#1}$	0.95	2.51	3.199(5)	129	1-x, 1-y, 1-z
C8-H8A···O2$^{\#3}$	0.99	2.49	3.297(6)	138	−1 + x, y, z
C13-H13···O10$^{\#1}$	0.95	2.57	3.242(5)	128	1-x, 1-y, 1-z
Complex **2**					
D–X···A	d(D–X)	d(X···A)	d(D···A)	∠D–X···A	Symmetry code
O8-H8···O11$^{\#1}$	0.88(3)	1.94(3)	2.801(4)	168(2)	1-x, 1-y, 1-z
O11$^{\#4}$-*H*11$^{\#4}$···O7	0.84	2.18	3.002(4)	168	-x, 2-y, 1-z
C9-H9AA···O3$^{\#5}$	0.99	2.56	3.221(4)	124	1-x, 1-y, 2-z
*C*2-H2···O10$^{\#1}$	0.95	2.55	3.208(3)	126	1-x, 1-y, 1-z
C8-H8A···O9	0.99	2.29	3.225(3)	158	
C13-H13···O1$^{\#1}$	0.95	2.60	3.367(3)	138	1-x, 1-y, 1-z
C15-H15···O11$^{\#4}$	0.95	2.54	3.329(4)	140	-x, 2-y, 1-z
C18-H18A···O10$^{\#1}$	0.99	2.39	3.379(3)	178	1-x, 1-y, 1-z
C22$^{\#6}$-H22B$^{\#6}$···O2	0.99	2.57	3.335(5)	134	x, 1 + y, z
Complex **3**					
D–X···A	d(D–X)	d(X···A)	d(D···A)	∠D–X···A	Symmetry code
O8-H8···O11	0.84	1.89	2.587	140	
O11-*H*11···O10$^{\#1}$	0.838	1.91	2.732	168	1-x, 1-y, 1-z
O2-H2···O10$^{\#1}$	0.95	2.56	3.259(3)	131	1-x, 1-y, 1-z
C8-H8A···O9	0.99	2.10	3.259(3)	158	
C9$^{\#10}$-H9B$^{\#10}$···O7$^{\#1}$	0.99	2.44	3.328(3)	148	-x, 1-y, 1-z
C13-H13···O1$^{\#1}$	0.95	2.47	3.282(3)	144	1-x, 1-y,1-z
C20-H20C···O11$^{\#5}$	0.98	2.44	3.379(4)	160	1-x, 1-y, 2-z

symmetry codes: $^{\#1}$ = 1-x, 1-y, 1-z; $^{\#2}$ = 1-x, 1-y, -z; $^{\#3}$ = -1 + x, y, z; $^{\#4}$ = -x, 2-y, 1-z; $^{\#5}$ = 1-x, 1-y, 2-z; $^{\#6}$ = x, 1 + y, z; $^{\#7}$ = x, 1-y, 1-z.

Table 4
Geometrical parameters for the π-related interactions for complexes.

Complex **1**					
D-O/H···A	D-O/H	O/H···A	D···A	∠D-O/H···A	Symmetry code
N1$^{\#2}$-O3$^{\#2}$···Cg1$^{\#1}$	1.249(5)	3.617(4)	4.163(5)	107.3(3)	1-x, 1-y, -z
C9$^{\#8}$-H9A$^{\#8}$···Cg2	0.990	2.95	3.634(5)	127	-x, 1-y, 1-z
Complex **2**					
D- H···A	D- H	H···A	D···A	∠D- H···A	Symmetry code
C9-H9AB···Cg2$^{\#9}$	0.990	2.86	3.801(3)	159	1-x, 2-y, 1-z
C19-H19C···Cg1	0.980	2.93	3.819(3)	151	
Complex **3**					
D- H···A	D- H	H···A	D···A	∠D- H···A	Symmetry code
C21-H21A···Cg2	0.980	2.96	3.598(3)	158	
C21-H21B···Cg1$^{\#5}$	0.980	2.91	3.649(3)	133	1-x, 1-y, 2-z
π···π	Rc[a]	R1v[b]	R2v[c]	α	Symmetry code
Cg2$^{\#10}$···Cg2$^{\#1}$	4.2228(13)	−3.3752(9)	−3.3752(9)	0.02(10)	-x,1-y,1-z

Cg1 is the centroids of the (C1-C6) rings, Cg2 is the centroids of the (C11-C16) rings. [a] Centroid distance between Cg I (Cg2$^{\#10}$) and Cg J (Cg2$^{\#1}$). [b] Vertical distance from ring centroid Cg 2$^{\#10}$ to ring Cg 2$^{\#1}$. [c] Vertical distance from ring centroid Cg 2$^{\#1}$ to ring Cg 2$^{\#10}$. α = dihedral angle between planes Cg2$^{\#10}$ and Cg2$^{\#1}$. Symmetry codes: $^{\#1}$ = 1-x, 1-y, 1-z; $^{\#2}$ = 1-x, 1-y, -z; $^{\#8}$ = -x, 1-y, 1-z; $^{\#9}$ = 1-x, 2-y, 1-z; $^{\#10}$ = -x, 1-y, 1-z.

intermolecular π-related interaction (C9-H9AB···Cg2$^{\#9}$) (Fig. 6) coordinate with five intermolecular hydrogen-bondings (O8-H8···O11$^{\#1}$, O11$^{\#4}$-*H*11$^{\#4}$···O7, C9-H9AA···O3$^{\#5}$, C15-H15···O11$^{\#4}$ and C22$^{\#6}$-H22B$^{\#6}$···O2) to form three-dimensional infinite supramolecular structure [1f,2g,24] (Fig. 7). Putative hydrogen bond interactions and geometrical parameters for the π-related interactions of complexes **1**–**3** are shown in Table 3 and Table 4, respectively.

*3.2.3. The crystal structure and supramolecular interactions of complex **3***

Complex **3** possesses inversion center and crystallizes in the triclinic crystal system, the formula is [{NiL(MeOH)(μ-OAc)}$_2$Ni]·2CH$_3$OH. The structure of complex **3** is similar to the former two (Fig. 8a, 8b). Ghosh group reported a trinuclear Ni(II) complex, the axial positions of Ni(II) atom in the center are coordination H_2O molecules, and the NCS^- ions coordinated in the axial positions of the terminal Ni(II) atoms are used as the counter-anion [3h]. The trinuclear Ni(II) structure reported by the Liu group in 2017, through the μ-$PhCOO^-$ ions to connect the metal Ni(II) atoms to form a new trinuclear Ni(II) complex [3i], there are different from that reported in this article.

By analyzing the intramolecular and intermolecular interactions, we found that there is a significant difference between complex **3** and the former two. Three intramolecular hydrogen bonds (*C*2-H2···O10$^{\#1}$, C8-H8A···O9 and C13-H13···O1$^{\#1}$) (Fig. 8c) were found in complex units, which is helpful to the unique structure of the complex. At the same time, four intermolecular hydrogen bonds (O8-H8···O11, O11-*H*11···O10$^{\#1}$, C9$^{\#10}$-H9B$^{\#10}$···O7$^{\#1}$ and C20-H20C···O11$^{\#5}$) (Fig. 9) coordinate with π-related interactions (C21-H21B···Cg1$^{\#5}$, C21-H21A···Cg2 and Cg2$^{\#10}$···Cg2$^{\#1}$) [1f,2g,24] (Fig. 10) to form two-dimensional infinite supramolecular structure. Through 2D fingerprints of quantitative analysis, complex **3** has more C··· C interactions, which is consistent with the supramolecular structures of the complexes [19a]. Putative hydrogen bond interactions and geometrical parameters for the

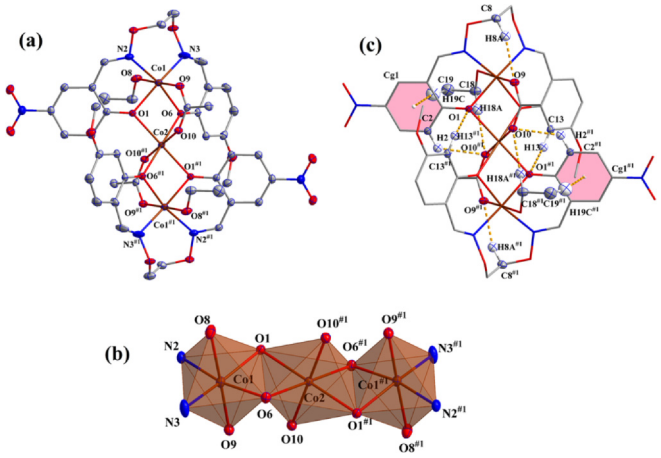

Fig. 5. (a) Molecule structure of complex **2**, ellipsoids are shown at the 30% probability level for reasons of clarity, symmetry code: #1 = 1-x, 1-y, 1-z. (b) Coordination polyhedrons for Co(II) atoms, symmetry code: #1 = 1-x, 1-y, 1-z. (c) View of the intramolecular hydrogen bonds and C19-H19C···Cg1 interactions (Cg1 are the centroids of atoms C1/C2/C3/C4/C5/C6.), symmetry code: #1 = 1-x, 1-y, 1-z. The disordered positions O atoms of O5 only show the more populated position for clarity. Hydrogen atoms and solvent molecules are omitted for clarity.

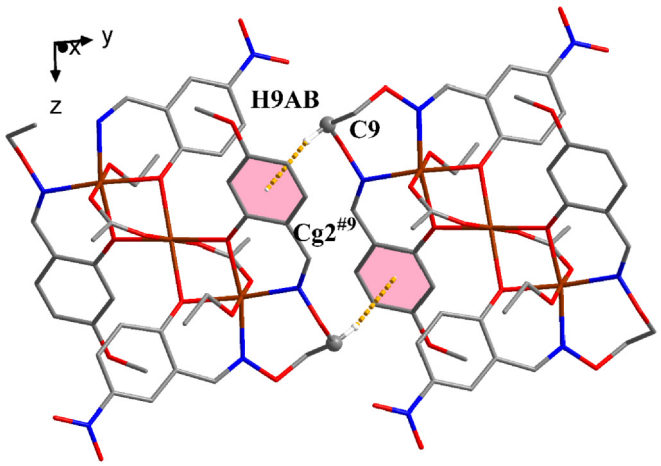

Fig. 6. View of the one-dimensional supramolecular structure of complex **2**. C9-H9AB···Cg2#9 interactions of complex **2** (Cg 2 is the centroids of atoms C11/C12/C13/C14/C15/C16.), symmetry code: #9 = 1-x, 2-y, 1-z. The disordered positions O atoms of O5 only show the more populated position and the hydrogen atoms and solvent molecules are omitted for clarity.

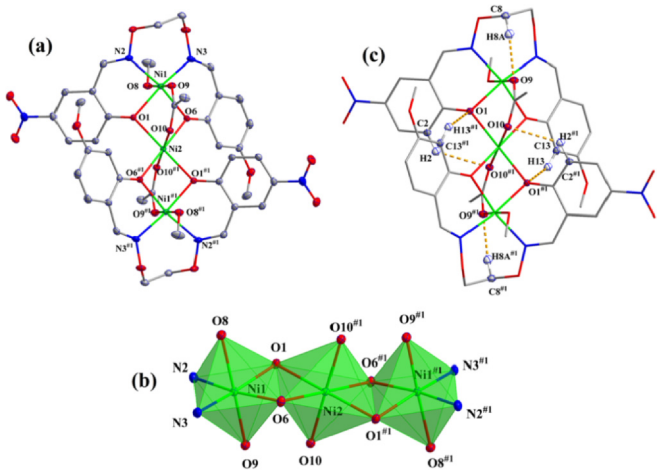

Fig. 8. (a) Molecule structure of complex **3**, ellipsoids are shown at the 30% probability level for reasons of clarity, symmetry code: #1 = 1-x, 1-y, 1-z. (b) Coordination polyhedrons for Ni(II) atoms, symmetry code: #1 = 1-x, 1-y, 1-z. (c) View of the intramolecular hydrogen bonds. Symmetry code: #1 = 1-x, 1-y, 1-z. Hydrogen atoms and solvent molecules are omitted for clarity.

π-related interactions of complexes **1**–**3** are shown in Table 3 and Table 4, respectively.

3.3. Hirshfeld surfaces analyses

In recent years, molecular crystal structure analysis using tools based on Hirshfeld surface has rapidly gained in popularity [20]. As a method for obtaining crystal stacking trend information, the derivation of the Hirshfeld surface and the decomposition of 2D fingerprints provide an intuitive and convenient method for quantitative analysis of the interactions in the crystal structure [21a]. The study of stacked patterns reveals the similarities and differences between related structures, provides great potential for the development of crystal engineering, and provides insight into the nature and strength of interactions between molecular crystal components [22]. We use CrystalExplorer to produce Hirshfeld surface and map parameters on them to analyze the intermolecular interactions [23].

The interactions between molecules were analyzed using the d_{norm} mapping on the Hirshfeld surface (Fig. 12a). The molecular surface showed a large dark red, indicating the existence of hydrogen bonds interactions [21b], at the same time, the interacting

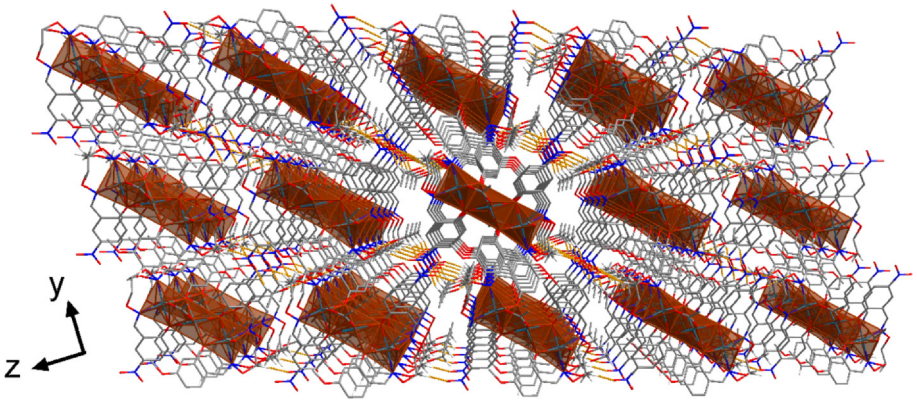

Fig. 7. The three-dimensional supramolecular structure of complex **2** is formed by intermolecular hydrogen bonds O8-H8···O11#1, O11#4-H11#4···O7, C9-H9AA···O3#5, C15-H15···O11#4 and C22#6-H22B#6···O2. Symmetry code: #1 = 1-x, 1-y, 1-z; #4 = -x, 2-y, 1-z; #5 = 1-x, 1-y, 2-z; #6 = x, 1 + y, z. The disordered positions O atoms of O5 only show the more populated position and the hydrogen atoms are omitted for clarity.

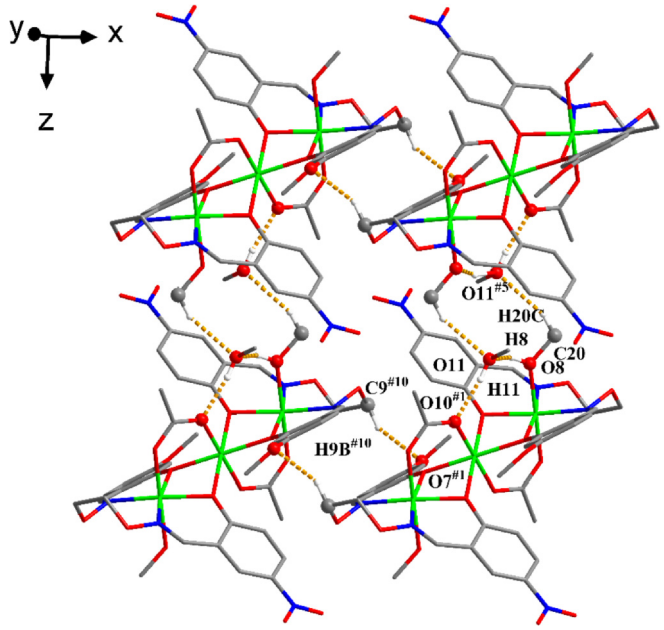

Fig. 9. The two-dimensional supramolecular structure of complex **3** is formed by intermolecular hydrogen bonds O8-H8···O11, O11-*H*11···O10$^{\#1}$, C9$^{\#10}$-H9B$^{\#10}$-···O7$^{\#1}$ and C20-H20C···O11$^{\#5}$, symmetry code: $^{\#1}$ = 1-x, 1-y, 1-z; $^{\#5}$ = 1-x, 1-y, 2-z; $^{\#10}$ = -x, 1-y, 1-z. Hydrogen atoms are omitted for clarity.

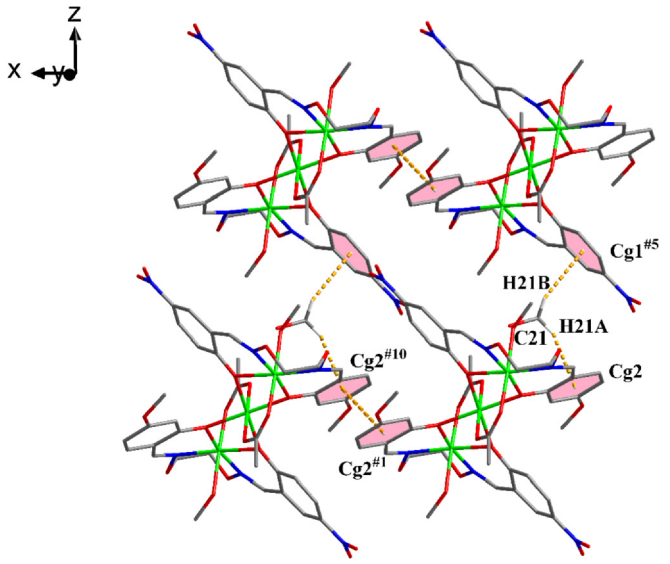

Fig. 10. The two-dimensional supramolecular structure of complex **3** is formed by C21-H21B··· Cg1$^{\#5}$, C21-H21A···Cg2 and Cg2$^{\#10}$···Cg2$^{\#1}$ and interactions, symmetry code: $^{\#1}$ = 1-x, 1-y, 1-z; $^{\#5}$ = 1-x, 1-y, 2-z; $^{\#10}$ = -x, 1-y, 1-z. Hydrogen atoms are omitted for clarity.

atoms from the neighboring molecules have been shown and marked in detail in Fig. 11, which corresponds to the supramolecular structures of the complexes **1**–**3**. The small area and light color on the d_{norm} indicated weak and longer interactions, rather than hydrogen bonds. Shape index is a qualitative measure of surface shape, red zones complement blue zones can be observed on the shape index of complexes **1**–**3**, which provided the expected equal triangles for the interactions between the aromatic rings (Fig. 12b) [19b], at the same time, there are large flat areas on curvedness of complexes **1**–**3** (Fig. 12c), they indicated the π···π stacking interactions in complex **1**–**3**, we can include C··· C interaction as an index of π···π stacking interaction [19b]. The ratio of intermolecular interactions that stabilize the crystal structure can be determined by analyzing the 2D fingerprint plot (Fig. 13) [24]. For complex **1**, H···H, O···H/H···O, C···H/H···C, C···O and C···C interactions are 42.4, 34.6, 14.2, 2.9 and 0.0%, respectively. For complex **2**, H···H, O···H/H···O, C···H/H···C, C···O and C···C interactions are 53.6, 29.5, 10.5, 2.5 and 0.7%, respectively. For complex **3**, H···H, O···H/H···O, C···H/H···C, C···O and C···C interactions are 47.6, 36.1, 10.6, 0.3 and 2.1%, respectively. Through quantitatively determined of the intermolecular interactions, we can find that the π···π stacking interactions in complexes **1**–**3** have obvious difference (**3** > **2** > **1**), there are consistent with the supramolecular structures of complex **1**–**3**. From the 2D fingerprint plot, we can find that H···H

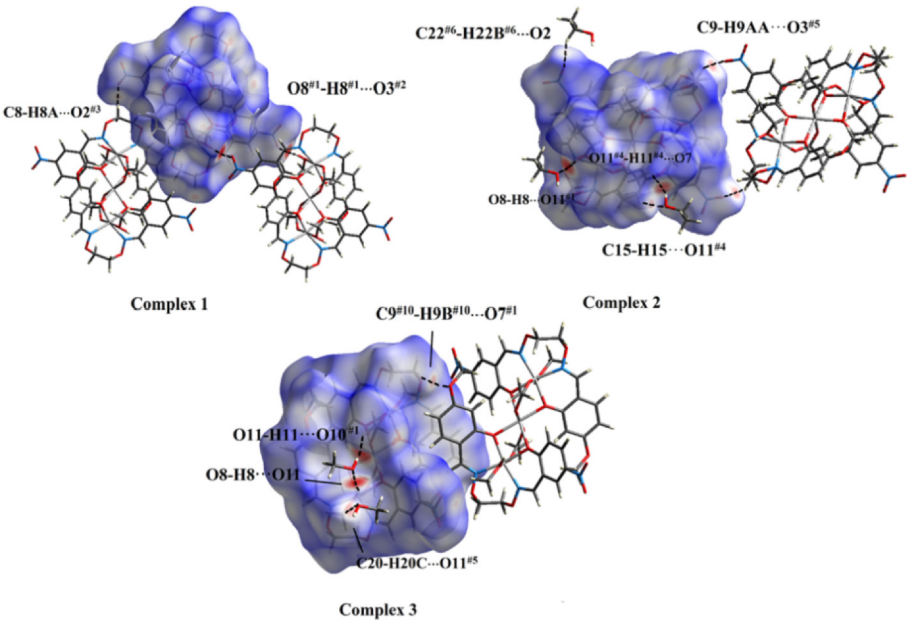

Fig. 11. d_{norm} surfaces of complexes **1**–**3**, the interacting atoms from the neighboring molecules have been shown and marked in detail, highlighting the hydrogen bonding motifs.

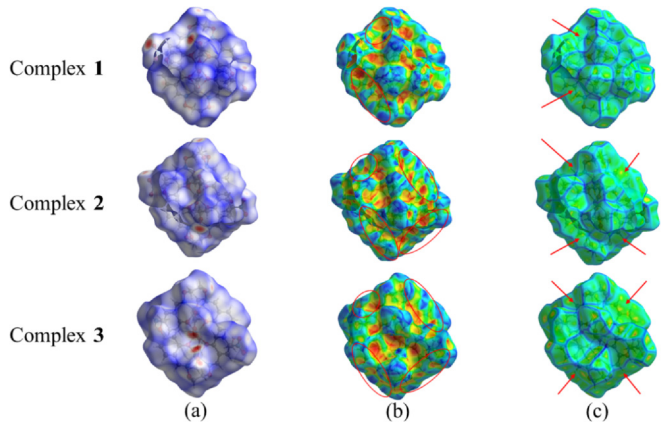

Fig. 12. Hirshfeld surfaces analyses mapped with (a) d_{norm}, (b) Shape index, (c) Curvedness of complexes **1**–**3**.

and O···H/H···O are the main interactions between the molecules of the complexes, which is mainly the effect of the oxygen atoms of the nitro groups, there is also confirmed in supramolecular structures, intermolecular interactions play key roles in the stacking mode of complexes **1**–**3**.

3.4. Fluorescence properties

The design and synthesis of optical (colorimetric and fluorescent) molecular probes have aroused great interest in a variety of scientific communities. In order to develop the related applications, salamo-based ligands and their complexes have been widely reported as chemical sensors [14a,15a,15b].

Fluorescence property experiments were performed in EtOH solution with the concentration of the ligand is 1×10^{-5} mol/L, at the same time, excitation wavelength is 280 nm, the titration curves of complexes **1**–**3** are depicted in Fig. 14. The strong emission band of the ligand was observed at about 325 nm, which is attributed to the π-π* charge transition of the ligand molecules [10a]. For complexes **1** and **2**, with the gradual addition of Co^{2+} (1×10^{-3} mol/L), the fluorescence intensity of the ligand decreased gradually, and the decreasing trend of the fluorescence intensity stopped when Co^{2+} ions were added to 1.5 equivalents (Fig. 14a) [9c,12c], The ligand H_2L as the signaling unit, when the metal atoms self-assemble with it, causing the excited state

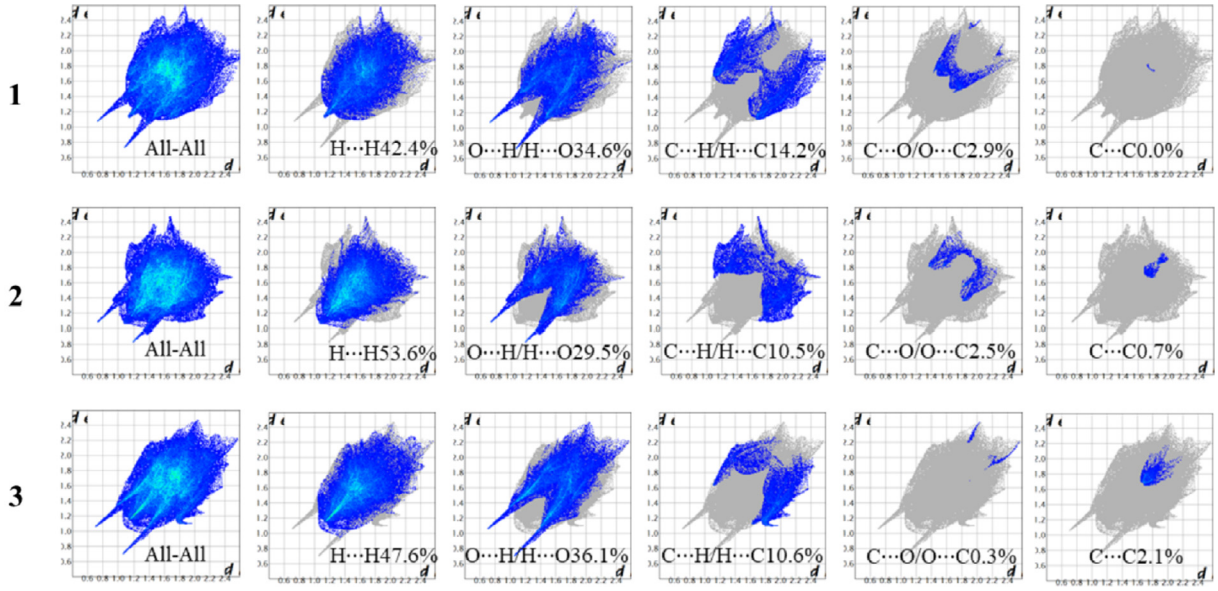

Fig. 13. The fingerprint plots for complexes **1**–**3** and the relative contributions of all contacts.

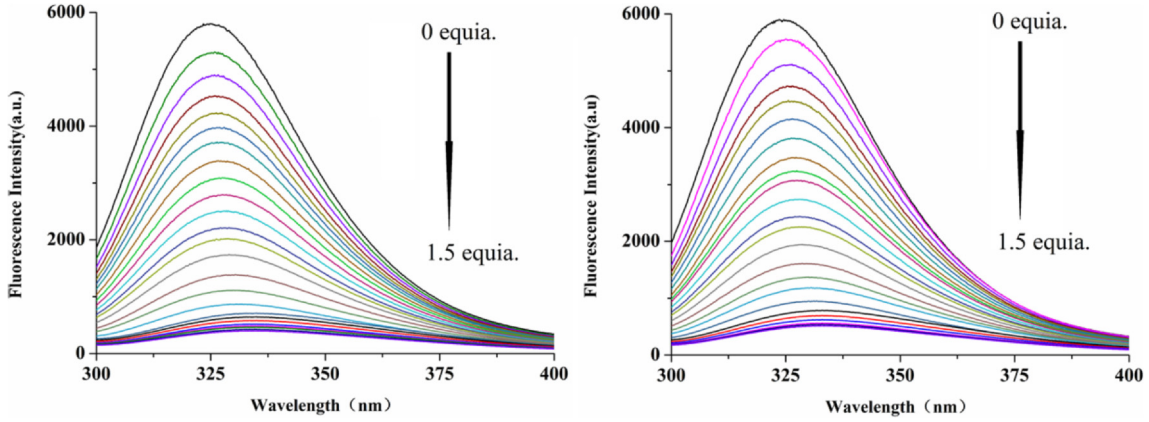

Fig. 14. (a) Fluorescence spectra of H_2L (1×10^{-5} M) with addition of various concentrations of Co^{2+} (1×10^{-3} M). (b) Fluorescence spectra of H_2L (1×10^{-5} M) with addition of various concentrations of Ni^{2+} (1×10^{-3} M).

electrons of the ligand transfer to the empty orbitals of the metal atoms (LMCT), which shows strong fluorescence quenching [13b,13d]. At the same time, the fluorescence of the Co^{2+} complexes have a red-shift of 7 nm relative to the ligand. The fluorescence titration curves of complex **3** are the same as that of the former two, the fluorescence of the Ni^{2+} complexes have a red-shift of 8 nm relative to the ligand (Fig. 14b).

4. Conclusion

Through wet-chemical method, three trinuclear complexes **1**–**3** were successfully synthesized, which belongs to $(L)^{3-}$: M(II) = 2:3 type homo-polynuclear complexes with inversion centers. The interactions of the complexes were quantitatively analyzed by Hirshfeld surface and 2D fingerprints, H···H and O···H/H···O are the main interactions between the molecules of the complexes, at the same time, π-π stacking interactions of complexes **1**–**3** are significantly different (**3** > **2** > **1**), meantime, the oxygen atoms of the nitro groups play important roles in the formation of intermolecular hydrogen bonds, which is consistent with the supramolecular structures of complexes **1**–**3**. The ligand H_2L has strong emission band at about 325 nm, but the complexes show strong fluorescence quenching and red-shift relative to the ligand.

Declaration of Competing Interest

The authors declare that they have no known competing financial interests or personal relationships that could have appeared to influence the work reported in this paper.

Acknowledgement

This work was supported by the National Natural Science Foundation of China (21761018), which is gratefully acknowledged.

References

[1] (a) S. Hrom, V. Sizov, O. Levin, A. Laaksonen, J. Phys. Chem. C. 125 (2020) 2926;
(b) A. Garous, S. Kasselouri, C. Mitsopouloub, J. Slettenc, C. Papadimitrioud, N. Hadjiliadisd, Polyhedron 18 (1999) 39;
(c) M. Damoc, A. Stoica, A. Macsim, M. Dascalu, M. Zaltariov, M. Cazacu, J. Mol. Liq. 316 (2020) 113852;
(d) M.M. Belmonte, E. Escudero-Adán, E. Martin, A. Kleij, Dalton Trans. 41 (2012) 5193;
(e) L.L. Liu, Q. Wang, C.J. Gao, H. Chen, W.S. Liu, Y. Tang, J. Phys. Chem. C 118 (2014) 14511;
(f) P. Manna, S. Seth, A. Das, J. Hemming, R. Prendergast, M. Helliwell, S. Choudhury, A. Frontera, S. Mukhopadhyay, Inorg. Chem. 51 (2012) 3557.
[2] (a) X.Y. Zou, B.W. Fei, G.M. Li, Polyhedron 192 (2020) 114811;
(b) W.Z. Huang, F.M. Tang, W.H. Hu, Y.C. Xu, W.W. Luo, Z.H. Hu, X.Y. Jia, D.Z. Wu, D.R. Gong, Mater. Today Commun. 26 (2021) 102068;
(c) Q. Wu, Y.F. Tang, Q.L. Zi, Polyhedron 166 (2019) 123;
(d) T. Gao, P.F. Yan, G.M. Li, G.F. Hou, J.S. Gao, Polyhedron 26 (2007) 5382;
(e) A. Finelli, V. Chabert, N. Hérault, A. Crochet, C. Kim, K. Fromm, Inorg. Chem. 58 (2019) 13796;
(f) P. Zhang, L. Zhang, S.Y. Lin, J.K. Tang, Inorg. Chem. 52 (2013) 6595;
(g) G.R. Desiraju, Acc. Chem. Res. 29 (1996) 441.
[3] (a) R. Kloditz, T. Radoske, M. Schmidt, T. Heine, T. Stumpf, M. Patzschke, Inorg. Chem. 60 (2021) 2514;
(b) N. Mohan, S.S. Sreejith, M.R.P. Kurup, Polyhedron 173 (2019) 114129;
(c) H. Kanso, R.M. Clarke, A. Kochem, H. Arora, C. Philouze, O. Jarjayes, T. Storr, F. Thomas, Inorg. Chem. 59 (2020) 5133;
(d) L.Z. Liu, M. Yu, X.Y. Li, Q.P. Kang, W.K. Dong, Chin. J. Inorg. Chem. 35 (2019) 1283;
(e) X.X. An, C. Liu, Z.Z. Chen, K.F. Xie, Y. Zhang, Crystals 9 (2019) 602;
(f) A. Datta, K. Das, C. Sen, N.K. Karan, J.H. Huang, C.H. Lin, E. Garribba, C. Sinha, T. Askun, P. Celikboyun, S.B. Mane, Spectrochim. Acta. A Mol. Biomol Spectrosc. 148 (2015) 427;
(g) M.I. Mocanu, A.A. Patrascu, M. Hillebrand, S. Shova, F. Lloret, M. Julve, M. Andruh, Eur. J. Inorg. Chem. 44 (2019) 4773;
(h) A. Das, K. Bhattacharya, S. Giri, A. Ghosh, Polyhedron 134 (2017) 295;
(i) M.Y. Liu, H.Y. Yu, Y.Q. Wang, Z.L. Liu, Inorg. Chem. Commun. 86 (2017) 281.
[4] (a) S.G. Robinson, X.Y. Wu, B.Y. Jiang, M.S. Sigman, S. Lin, J. Am. Chem. Soc. 142 (2020) 18471;
(b) C.B. Provis-Evans, S. Lau, V. Krewald, R. Webster, ACS Catal. 10 (2020) 10157;
(c) A. Gaston, Z. Greindl, C. Morrison, J. Garden, Inorg. Chem. 60 (2021) 2294;
(d) Y.X. Sun, Y.Q. Pan, X.X.Y. Zhang, Crystals 9 (2019) 607;
(e) A. Das, S. Goswami, R. Sen, A. Ghosh, Inorg. Chem. 58 (2019) 5787;
(f) S. Maity, P. Mahapatra, T. Ghosh, R. Gomila, A. Frontera, A. Ghosh, Dalton Trans. 50 (2021) 4686.
[5] (a) G.N. Liu, R.Y. Zhao, R.D. Xu, X. Zhang, X.N. Tang, Q.J. Dan, Y.W. Wei, Y.Y. Tu, Q.B. Bo, C.C. Li, Cryst. Growth Des. 18 (2018) 5441;
(b) G.N. Liu, R.D. Xu, R.Y. Zhao, Y.Q. Sun, Q.B. Bo, Z.Y. Duan, Y.H. Li, Y.Y. Wang, Q. Wu, C.C. Li, ACS Sustainable Chem. Eng. 7 (2019) 18863;
(c) X.Y. Zou, C.Y. Du, Y.P. Dong, G.M. Li, Inorg. Chim. Acta 512 (2020) 119860;
(d) P. Milbeo, F. Quintin, L. Moulat, C. Didierjean, J. Martinez, X. Bantreil, M. Calmès, F. Lamaty, Tetrahedron Lett. 63 (2021) 152706;
(e) M. Strianese, D. Guarnieri, M. Lamberti, A. Landi, A. Peluso, C. Pellecchia, Inorg. Chem. 59 (2020) 15977;
(f) S. Hossain, K. Singh, A. Lakma, R. Pradhan, A. Singh, Sens Actuators B Chem. 239 (2017) 1109;
(g) X.J. Wang, Y.X. Jiang, Y.F. Chen, S.S. Yu, D. Shi, F. Zhao, Y. Chen, Y.L. Wang, B. Y. Huo, X.Q. Yu, L. Pu, J. Org. Chem. 85 (2020) 4901.
[6] (a) X. Xu, Y.J. Li, T. Feng, W.K. Dong, Y.J. Ding, Lumin. 36 (2021) 169;
(b) Y.D. Peng, R.Y. Li, P. Li, Y.X. Sun, Crystals 11 (2021) 113;
(c) S. Lee, N. Shin, S. Kwak, K. Hyun, W. Woo, J. Lee, H. Hwang, M. Kim, J. Lee, Y. Kim, K. Lee, M. Park, Inorg. Chem. 56 (2017) 2621;
(d) Z.Q. Zhou, Y.X.M.X. Li, E.N. Nfor, Z.X. Wang, Cryst. Growth Des. 20 (2020) 5760;
(e) S. Akine, M.a. Miyashita, T. Nabeshima, Chem. Eur. J. 25 (2019) 1432.
[7] S. Akine, T. Nabeshima, Dalton Trans. 47 (2009) 10395.
[8] (a) S. Akine, T. Taniguchi, T. Nabeshima, Chem. Lett. 30 (2001) 682;
(b) S. Akine, T. Taniguchi, T. Nabeshima, Angew. Chem. 42 (2002) 4670;
(c) D.W. Dixon, R.H. Weiss, J. Org. Chem. 49 (1984) 4487.
[9] (a) X. Xu, T. Feng, S.S. Feng, W.K. Dong, Appl. Organomet. Chem. 35 (2021) e6057;
(b) J.F. Wang, R.N. Bian, T. Feng, K.F. Xie, L. Wang, Y.J. Ding, Microchem. J. 160 (2021) 105676;
(c) C. Liu, Z.L. Wei, H.R. Mu, W.K. Dong, Y.J. Ding, J. Photochem. Photobio. A 397 (2020) 112569.
[10] (a) P. Li, G.X. Yao, M. Li, W.K. Dong, Polyhedron 195 (2021) 114981;
(b) R.N. Bian, J.F. Wang, X. Xu, X.Y. Dong, Y.J. Ding, Appl. Organomet. Chem. 35 (2021) e6040;
(c) M. Yu, Y. Zhang, Y.Q. Pan, L. Wang, Inorg. Chim. Acta 509 (2020) 119701.
[11] C. Liu, X.X. An, Y.F. Cui, K.F. Xie, W.K. Dong, Appl. Organomet. Chem. 34 (2020) e5272.
[12] (a) Y.F. Cui, C. Liu, Y. Zhang, Y. Zhang, Inorg. Nano-Met. Chem. 51 (2021) 288;
(b) X.X. An, Z.Z. Chen, H.R. Mu, L. Zhao, Inorg. Chim. Acta 511 (2020) 119823;
(c) Y. Zhang, M. Yu, Y.Q. Pan, Y. Zhang, L. Xu, X.Y. Dong, Appl. Organomet. Chem. 34 (2020) e5442;
(d) Y. Zhang, Y.J. Li, S.Z. Guo, T. Fu, L. Zhao, Transit. Met. Chem. 45 (2020) 485.
[13] (a) Y.Q. Pan, Y. Zhang, M. Yu, Y. Zhang, L. Wang, Appl. Organomet. Chem. 34 (2020) e5441;
(b) L. Wang, Y.Q. Pan, J.F. Wang, Y. Zhang, Y.J. Ding, J. Photochem. Photobio. A 400 (2020) 112719;
(c) X. Xu, J.F. Wang, R.N. Bian, L. Zhao, J. Coord. Chem. 73 (2020) 2209;
(d) Y.D. Peng, Y. Zhang, Y.L. Jiang, Z.L. Ren, F. Wang, L. Wang, J. Fluores. 30 (2020) 1049.
[14] (a) S. Li, X.X. An, J.F. Wang, L. Wang, L.G. Xue, J. Struct. Chem. 61 (2020) 1993;
(b) M. Yu, H.R. Mu, L.Z. Liu, N. Li, Y. Bai, X.Y. Dong, Chinese J. Inorg. Chem. 35 (2019) 1109;
(c) T. Feng, J.F. Wang, L.L. Li, Y. Zhang, X.Y. Dong, J. Struct. Chem. 62 (2021) 415.
[15] (a) H.R. Mu, M. Yu, L. Wang, Y. Zhang, Y.J. Ding, Phosphorus Sulfur Silicon Relat. Elem. 195 (2020) 730;
(b) R.Y. Li, Z.L. Wei, L. Wang, Y. Zhang, J.X. Ru, Microchem. J. 162 (2021) 105720.
[16] (a) S. Akine, S. Hotate, T. Matsumoto, T. Nabeshima, Chem. Commun. 47 (2011) 2925;
(b) S. Akine, S. Hotate, T. Nabeshima, J. Am. Chem. Soc. 133 (2011) 13868;
(c) S. Akine, T. Matsumoto, T. Nabeshima, Angew. Chem. 128 (2016) 972.
[17] G.M. Sheldrick, Acta Cryst. A71 (2015) 3.
[18] (a) G.M. Sheldrick, Acta Cryst. C71 (2015) 3;
(b) O.V. Dolomanov, L.J. Bourhis, R.J. Gildea, J.A.K. Howard, H. Puschmann, J. Appl. Cryst. 42 (2009) 339;
(c) L. Krause, R. Herbst-Irmer, G.M. Sheldrick, D. Stalke, J. Appl. Cryst. 48 (2015) 3.
[19] (a) E. Jaime-Adán, J.M. Germán-Acacio, R.A. Toscano, S. Hernández-Ortega, J. Valdés-Martínez, Cryst. Growth Des. 20 (2020) 2240;
(b) C.B. Pinto, L.H.R.D. Santos, B.L. Rodrigues, Acta Cryst C75 (2019) 707.
[20] S.K. Seth, Acta Cryst. E 74 (2018) 600.
[21] (a) K. Takahashi, N. Hoshino, T. Takeda, S. Noro, T. Nakamura, S. Takeda, T. Akutagawa, Inorg. Chem. 54 (2015) 9423;
(b) S. Banerjeea, P. Ghoraia, P. Sarkarb, A. Panjac, A. Saha, Inorg. Chim. Acta 499 (2020) 119176.
[22] M. Spackman, D. Jayatilaka, CrystEngComm 11 (2009) 19.
[23] S.K. Seth, G.C. Maity, T. Kar, J. Mol. Struct. 1000 (2011) 120.
[24] P. Manna, S.K. Seth, M. Mitra, A. Das, N.J. Singh, S.R. Choudhury, T. Kar, S. Mukhopadhyay, CrystEngComm 15 (2013) 7879.